

DEEP RELAXATION: PARTIAL DIFFERENTIAL EQUATIONS FOR OPTIMIZING DEEP NEURAL NETWORKS

PRATIK CHAUDHARI^{1*}, ADAM OBERMAN^{2*}, STANLEY OSHER³, STEFANO SOATTO¹, AND GUILLAME CARLIER⁴

¹ Computer Science Department, University of California, Los Angeles.

² Department of Mathematics and Statistics, McGill University, Montreal.

³ Department of Mathematics & Institute for Pure and Applied Mathematics, University of California, Los Angeles.

⁴ Mathématiques Appliquées, Université Paris IX Dauphine.

Email: pratikac@ucla.edu, adam.oberman@mcgill.ca, sjo@math.ucla.edu, soatto@ucla.edu, carlier@ceremade.dauphine.fr

Abstract: We establish connections between non-convex optimization methods for training deep neural networks (DNNs) and the theory of partial differential equations (PDEs). In particular, we focus on relaxation techniques initially developed in statistical physics, which we show to be solutions of a nonlinear Hamilton-Jacobi-Bellman equation. We employ the underlying stochastic control problem to analyze the geometry of the relaxed energy landscape and its convergence properties, thereby confirming empirical evidence. This paper opens non-convex optimization problems arising in deep learning to ideas from the PDE literature. In particular, we show that the non-viscous Hamilton-Jacobi equation leads to an elegant algorithm based on the Hopf-Lax formula that outperforms state-of-the-art methods. Furthermore, we show that these algorithms scale well in practice and can effectively tackle the high dimensionality of modern neural networks.

Keywords: Non-convex optimization, deep learning, neural networks, partial differential equations, stochastic gradient descent, local entropy, regularization, smoothing, local convexity, optimal control, proximal, inf-convolution

1. INTRODUCTION

Deep Neural Networks (DNNs) have achieved remarkable success in a number of applied domains from visual recognition and speech, to natural language processing and robotics (LeCun et al., 2015). Despite many attempts, an understanding of the roots of this success remains elusive. DNNs are a parametric class of functions whose parameters are found by minimizing a non-convex loss, typically via stochastic gradient descent (SGD), with a variety of explicit or implicit regularizers. In this paper, we establish connections between optimization techniques for deep neural networks and partial differential equations (PDEs).

1.1. Overview of main mathematical results. Given a loss function $f(x)$, we first motivate our results by studying a new function called *local entropy* $f_\gamma(x)$ which was recently introduced by Baldassi et al. (2015) and was shown to be effective in training deep networks by Chaudhari et al. (2016).

Our first result in Sec. 3 gives a *PDE interpretation of local entropy*. We observe that $f_\gamma(x)$ is the solution of a nonlinear, viscous Hamilton-Jacobi (HJ) PDE. Using semiconcavity, this observation immediately leads to regularity results for the solutions that are consistent with empirical observations. The viscous HJ equation is characterized as the value function of a stochastic optimal control problem in Sec. 4. This helps us *prove an improvement in the expected loss over SGD* in Theorem 8. Moreover, we *quantify the improvement* in terms of the integral of the norm of the gradient along the path. This result is based on well-known techniques from stochastic control theory (Fleming and Soner, 2006) and the comparison principle for viscosity solutions. We are not aware of other results in deep learning of this nature.

Chaudhari et al. (2016) compute the gradient of local entropy $\nabla f_\gamma(x)$ using an auxiliary stochastic differential equation (SDE). Sec. 6 builds upon this and derives local entropy using homogenization of SDEs (Pavliotis and Stuart, 2008). Using similar techniques, we *prove that the Elastic-SGD algorithm (Zhang et al., 2015) is equivalent to local entropy*. The equivalence is a surprising result, since the former runs by computing temporal averages on a single processor while the latter computes an average of coupled independent realizations of SGD over multiple processors. Again, we are able to use well-understood mathematical results to make this connection; in this case, we use ergodicity. Tools from optimal

* Joint first authors.

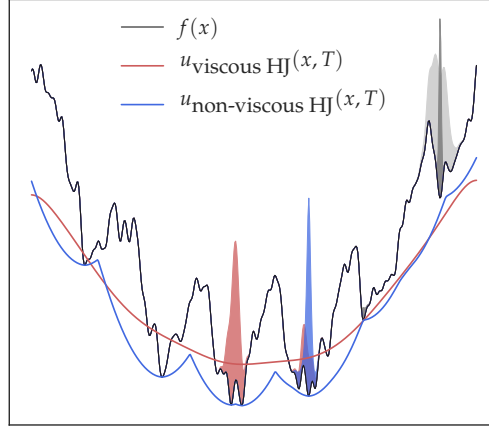


FIGURE 1. One dimensional loss function $f(x)$ (black) and smoothing of $f(x)$ by the viscous Hamilton-Jacobi equation (red) and the non-viscous Hamilton Jacobi equation (blue). The initial density (light grey) is evolved using the Fokker-Planck equation (29) which uses solutions of the respective PDEs. The terminal density obtained using SGD (dark grey) remains concentrated in a local minimum. The function $u_{\text{viscous HJ}}(x, T)$ (red) is convex, with the global minimum close to that of $f(x)$, consequently the terminal density (red) is concentrated near the minimum of $f(x)$. The function $u_{\text{non-viscous HJ}}(x, T)$ (blue) is nonconvex, so the presence of gradients pointing away from the global minimum slows down the evolution. Nevertheless, the corresponding terminal density (blue) is concentrated in a nearly optimal local minimum. Note that $u_{\text{non-viscous HJ}}(x, T)$ is a generalized convex envelope of f : it is given by the Hopf-Lax formula (HL), which is the envelope of parabolas with a fixed curvature at each point on the graph of $f(x)$. Also note that both the value and location of some local extrema for non-viscous HJ are unchanged and the regions of convexity widen. On the other hand, local maxima located in smooth concave regions see their concave region shrink, disappear and the maximal value eventually diminishes. This figure was produced by solving (29) using monotone finite differences (Oberman, 2006).

transportation (Santambrogio, 2015) imply that there is a threshold parameter related to the semiconvexity of $f(x)$ for which the *auxiliary SGD converges exponentially*. Beyond this threshold, the auxiliary problem is non-convergent; this is discussed in Remark 17 in Sec. 4.

Our next results have significant algorithmic implications. The benefits of using $f_\gamma(x)$ instead of $f(x)$ in the optimization do not depend on the coefficient of viscosity in the PDE. In Sec. 5, we exploit this to study the non-viscous Hamilton-Jacobi (HJ) equation

$$u_t = -\frac{1}{2} |\nabla u|^2,$$

and obtain a *simpler and significantly more effective* algorithm. Indeed, it is a known result that solutions of the viscous HJ equation converge to solutions of the non-viscous case in the limit as the viscosity goes to zero (Evans, 1998). Moreover, using the Hopf-Lax formula, the gradient $p^* = \nabla u(x, t)$ can be elegantly computed as the fixed point

$$p^* = \nabla f(x - tp^*).$$

The smoothing performed by the non-viscous HJ equation *preserves local minima* of $f(x)$ for short times, which is an important property for optimization and machine learning. For small times, we show using semiconcavity that these solutions quickly *widen the convex regions* in the energy landscape (cf. Sec. 7). Moreover, as Fig. 1 shows, local maxima belonging to smooth concave regions see their *concave regions shrink* and eventually disappear with a corresponding decrease in the maximal value.

The above approach is particularly interesting because the Hopf-Lax formula is equivalent to inf-convolution, which is a standard technique in convex analysis via Moreau envelopes (Moreau, 1965; Bauschke and Combettes, 2011). The gradient is obtained using the proximal operator which is, again, a key tool in modern optimization. While smoothing by the heat equation becomes increasingly expensive as the dimensionality grows, inf-convolution *does not suffer from the curse of dimensionality*. In fact, iterating inf and sup convolutions is an effective smoothing method in arbitrary dimensions (Lasry and Lions, 1986). We compared our techniques with the smoothing performed by the heat equation in Sec. 6.3 and also provide an empirical comparison in Sec. 8.

2. BACKGROUND

2.1. Deep neural networks (DNNs). A deep network is a nested composition of linear functions of an input datum $\xi \in \mathbb{R}^d$ and a nonlinear function σ at each level. The output of a DNN, denoted by $y(x; \xi)$, can be written as

$$y(x; \xi) = \sigma' \left(x^p \sigma \left(x^{p-2} \dots \sigma \left(x^1 \xi \right) \dots \right) \right); \quad (1)$$

where $x^1, \dots, x^{p-1} \in \mathbb{R}^{d \times d}$ and $x^p \in \mathbb{R}^{d \times K}$ are the parameters or “weights” of the network. We will let $x \in \mathbb{R}^n$ denote their concatenation after rearranging each one of them as a vector. The functions $\sigma(\cdot)$ are applied point-wise to each element of their argument. For instance, in a network with rectified linear units (ReLUs), we have $\sigma(z) = \max(0, z)$ for $z \in \mathbb{R}^d$. Typically, the last non-linearity is set to $\sigma'(z) = \mathbf{1}_{\{z \geq 0\}}$. A DNN is thus a function with n parameters that produces an output $y(x; \xi) \in \{1, \dots, K\}$ for each input ξ .

In supervised learning or “training” of a deep network for the task of image classification, given a finite sample of inputs and outputs $D = \{\xi^i, y^i\}_{i=1}^N$ (dataset), one wishes to minimize the empirical loss¹

$$f(x) := \frac{1}{N} \sum_{i=1}^N f_i(x); \quad (2)$$

where $f_i(x)$ is a loss function that measures the discrepancy between the predictions $y(x, \xi^i)$ for the sample ξ^i and the true label y^i . For instance, the zero-one loss is

$$f_i(x) := \mathbf{1}_{\{y(x; \xi^i) \neq y^i\}}.$$

Another typical choice of classification loss is cross-entropy, whereas for regression the loss could be a quadratic penalty $f_i(x) := \frac{1}{2} \|y(x; \xi^i) - y^i\|_2^2$. Regardless of the choice of the loss function, **the overall objective $f(x)$ in deep learning is a non-convex function of its argument x .**

In the sequel, we will dispense with the specifics of the loss function and consider training a deep network as a generic non-convex optimization problem given by

$$x^* = \arg \min_x \frac{1}{N} \sum_{i=1}^N f_i(x). \quad (3)$$

However, the particular relaxation and regularization schemes we describe are developed for, and tested on, classification tasks using deep networks.

2.2. Stochastic gradient descent (SGD). First-order methods are the default choice for optimizing (3), since the dimensionality of x is easily in the millions. Furthermore, typically, one cannot compute the entire gradient $N^{-1} \sum_{i=1}^N \nabla f_i(x)$ at each iteration (update) because N can also be in the millions for modern datasets.² Stochastic gradient descent (Robbins and Monro, 1951) consists of performing partial computations of the form

$$x^{k+1} = x^k - \eta_k \nabla f_{i_k}(x^{k-1}) \quad \text{where } \eta_k > 0, k \in \mathbb{N} \quad (4)$$

where i_k is sampled uniformly at random from the set $\{1, \dots, N\}$, at each iteration, starting from a random initial condition x^0 . The stochastic nature of SGD arises from the approximation of the gradient using only a subset of data points. One can also average the gradient over a *set* of randomly chosen samples, called a “mini-batch”. With an abuse of notation, we denote the gradient on such a mini-batch by $\nabla f_{i_k}(x)$ as well.

If each $f_i(x)$ is convex and the gradient $\nabla f_i(x)$ is uniformly Lipschitz, SGD converges at a rate

$$\mathbb{E} \left[f(x^k) \right] - f(x^*) = \mathcal{O}(k^{-1/2});$$

this can be improved to $\mathcal{O}(k^{-1})$ using additional assumptions such as strong convexity (Nemirovski et al., 2009) or at the cost of memory, e.g., SAG (Schmidt et al., 2013), SAGA (Defazio et al., 2014) among others. One can also obtain

¹The empirical loss is a sample approximation of the expected loss, $\mathbb{E}_{x \sim P} f(x)$, which cannot be computed since the data distribution P is unknown. The extent to which the empirical loss (or a regularized version thereof) approximates the expected loss relates to generalization, i.e., the value of the loss function on (“test” or “validation”) data drawn from P but not part of the training set D .

²For example, the ImageNet dataset (Krizhevsky et al., 2012) has $N = 1.25$ million RGB images of size 224×224 (i.e. $d \approx 10^5$) and $K = 1000$ distinct classes. A typical model, e.g. the Inception network (Szegedy et al., 2015) used for classification on this dataset has about $N = 10$ million parameters and is trained by running (4) for $k \approx 10^5$ updates; this takes roughly 100 hours with 8 graphics processing units (GPUs).

convergence rates that scale as $\mathcal{O}(k^{-1/2})$ for non-convex loss functions if the stochastic gradient is unbiased with bounded variance (Ghadimi and Lan, 2013).

2.3. SGD in continuous time. Developments in this paper hinge on interpreting SGD as a continuous-time stochastic differential equation. As is customary (Ghadimi and Lan, 2013), we assume that the stochastic gradient $\nabla f_{i_k}(x^{k-1})$ in (4) is unbiased with respect to the full-gradient and has bounded variance, i.e., for all $x \in \mathbb{R}^n$,

$$\begin{aligned}\mathbb{E}[\nabla f_{i_k}(x)] &= \nabla f(x), \\ \mathbb{E}[\|\nabla f_{i_k}(x) - \nabla f(x)\|^2] &\leq 2\beta^{-1};\end{aligned}$$

for some $\beta > 0$. The discrete-time dynamics in (4) can then be modeled by a stochastic differential equation (Pavliotis and Stuart, 2008)

$$dx(t) = -\nabla f(x(t)) dt + \sqrt{2\beta^{-1}} dW(t); \quad (\text{SGD})$$

for $t \geq 0$ where $W(t) \in \mathbb{R}^n$ is the n -dimensional Wiener process. The generator, \mathcal{L} , corresponding to (4) is defined for smooth functions ϕ as

$$\mathcal{L}\phi = -\nabla f \cdot \nabla \phi + \beta^{-1} \Delta \phi. \quad (5)$$

The adjoint operator \mathcal{L}^* is given by $\mathcal{L}^*\rho = \nabla \cdot (\nabla f \rho) + \beta^{-1} \Delta \rho$. Given the function $V(x) : X \rightarrow \mathbb{R}$, define

$$u(x, t) = \mathbb{E}[V(x(T))] = \mathbb{E}[x(T) \mid x(t) = x] \quad (6)$$

to be the expected value of V at the final time for the path (SGD) with initial data $x(t) = x$. By taking expectations in the Itô formula, it can be established that u satisfies the backward Kolmogorov equation

$$\frac{\partial u}{\partial t} = \mathcal{L}u, \quad \text{for } t < s \leq T,$$

along with the terminal value $u(x, T) = V(x)$. Furthermore, $\rho(x, t)$, the probability density of $x(t)$ at time t , satisfies the forward Kolmogorov or the Fokker-Planck equation (Risken, 1984)

$$\frac{\partial}{\partial t} \rho(x, t) = \nabla \cdot (\nabla f(x) \rho(x, t)) + \beta^{-1} \Delta \rho(x, t) \quad (\text{FP})$$

along with the initial condition $\rho(x, 0) = \rho_0(x)$ which represents the probability density of the initial distribution. With mild assumptions on $f(x)$, and even when f is non-convex, $\rho(x, t)$ converges to the unique stationary solution of (FP) as $t \rightarrow \infty$. Elementary calculations show that the stationary solution is the Gibbs distribution

$$\rho^\infty(x; \beta) = Z(\beta)^{-1} e^{-\beta f(x)}, \quad (7)$$

for a normalizing constant $Z(\beta)$. The parameter $\beta > 0$ is known as inverse temperature in the physics literature and we can see from (7) that as $\beta \rightarrow \infty$, the Gibbs distribution ρ^∞ concentrates on the global minimizers of $f(x)$.

The celebrated paper (Jordan et al., 1998) interpreted the Fokker-Planck equation as a gradient flow in the Wasserstein metric d_{W_2} (Santambrogio, 2015) and obtained the rate of convergence of (FP) to its stationary distribution. If we define

$$J(\rho) = \int_{\mathbb{R}^n} f(x) \rho dx + \beta^{-1} \int \rho \log \rho dx;$$

for a λ -convex $f(x)$, i.e., $\nabla^2 f(x) \geq \lambda$, the solution $\rho(x, t)$ converges exponentially with rate λ to ρ^∞ (Carrillo et al., 2006),

$$d_{W_2}(\rho(x, t), \rho^\infty) \leq d_{W_2}(\rho(x, 0), \rho^\infty) e^{-\lambda t}. \quad (8)$$

Remark 1. The solutions of a linear Fokker-Planck equation are stable (Evans, 1998). If $\tilde{f}(x)$ is a small perturbation of a λ -convex function $f(x)$, solutions to (FP) with f and \tilde{f} remain close. This stability suggests exponential convergence to the steady solution even for small perturbations of λ -convex functions.

Under mild assumptions for non-convex functions $f(x)$, the Gibbs distribution ρ^∞ is still the unique steady solution of (FP). However, convergence of $\rho(x, t)$ can take an exponentially long time. Such dynamics are said to exhibit ‘‘metastability’’ (Bovier and den Hollander, 2006), i.e., there may be multiple measures which are stable on time scales of order one. Kramers’ formula (Kramers, 1940) for Brownian motion in a double-well potential is the simplest example of such a phenomenon: if $f(x)$ is a double-well with two local minima at locations $x_1, x_2 \in \mathbb{R}$ with a saddle point $x_3 \in \mathbb{R}$ connecting them, we have

$$\mathbb{E}_{x_1}[\tau_{x_2}] \propto \frac{1}{|f''(x_3) f''(x_1)|^{1/2}} \exp(\beta(f(x_3) - f(x_1)));$$

where τ_{x_2} is the time required to transition from x_1 to x_2 under the dynamics in (SGD). The one dimensional example can be generalized to the higher dimensional case (Bovier and den Hollander, 2006). Observe that there are two terms that contribute to the slow time scale: (i) the denominator involves the Hessian at a saddle point x_3 , and (ii) the exponential dependence on the difference of the energies $f(x_1)$ and $f(x_2)$. In the higher dimensional case the first term can also go to infinity if the spectral gap goes to zero.

Simulated annealing (Kushner, 1987; Chiang et al., 1987) is a popular technique which aims to evade metastability and locate the global minimum of a general non-convex $f(x)$. The key idea is to control the variance of the Wiener process, in particular, decrease it exponentially slowly as

$$dx(t) = -\nabla f(x(t)) dt + \sqrt{\frac{2}{\log(t+1)}} dW(t). \quad (9)$$

There are theoretical results that prove that simulated annealing converges to the global minimum (Geman and Hwang, 1986); however the time required is still exponential.

2.4. SGD heuristics in deep learning. State-of-the-art results in deep learning leverage a number of heuristics. Variance reduction of the stochastic gradients of Sec. 2.2 leads to improved theoretical convergence rates for convex loss functions (Schmidt et al., 2013; Defazio et al., 2014) and is implemented in algorithms such as AdaGrad (Duchi et al., 2011), Adam (Kingma and Ba, 2014) etc.

Adapting the step-size, i.e., changing η_k in (4) with time k , is common practice. But while classical convergence analysis suggests step-size reduction of the form $\mathcal{O}(k^{-1})$ (Robbins and Monro, 1951; Schmidt et al., 2013), staircase-like drops are more commonly used. Merely adapting the step-size is not equivalent to simulated annealing, which explicitly modulates the diffusion term. This can be achieved by modulating the mini-batch size i_k in (4). Note that as the mini-batch size goes to N and the step-size η_k is $\mathcal{O}(N)$, the stochastic term in (9) vanishes (Li et al., 2015).

2.5. Regularization of the loss function. A number of prototypical models of deep neural networks have been used in the literature to analyze characteristics of the energy landscape. If one foregoes the nonlinearities, a deep network can be seen as a generalization of principal component analysis (PCA), i.e., as a matrix factorization problem; this is explored by Baldi and Hornik (1989); Haeffele and Vidal (2015); Soudry and Carmon (2016); Saxe et al. (2014), among others. Based on empirical results such as Dauphin et al. (2014), authors in Bray and Dean (2007); Fyodorov and Williams (2007); Choromanska et al. (2015) and Chaudhari and Soatto (2015) have modeled the energy landscape of deep neural networks as a high-dimensional Gaussian random field. In spite of these analyses being drawn from vastly diverse areas of machine learning, they suggest that, in general, the energy landscape of deep networks is highly non-convex and rugged.

Smoothing is an effective way to improve the performance of optimization algorithms on such a landscape and it is our primary focus in this paper. This can be done by convolution with a kernel (Chen, 2012); for specific architectures this can be done analytically Mobahi (2016) or by averaging the gradient over random, local perturbations of the parameters (Gulcehre et al., 2016). In the following section, we introduce a technique for smoothing that has shown good empirical performance. We compare and contrast the above mentioned smoothing techniques in a unified mathematical framework in this paper.

3. LOCAL ENTROPY AND THE VISCOUS HAMILTON-JACOBI PDE

Local entropy is a modified loss function first introduced as a means for studying the energy landscape of the discrete perceptron, i.e., a “shallow” neural network with one layer and discrete parameters, e.g., $x \in \{-1, 1\}^n$ (Baldassi et al., 2016b). An analysis of local entropy using the replica method (Mezard et al., 1987) predicts dense clusters of solutions to the optimization problem (3). Parameters that lie within such clusters yield better error on samples outside the training set D , i.e., they “generalize” well (Baldassi et al., 2015).

Recent papers by Baldassi et al. (2016a) and Chaudhari et al. (2016) have suggested algorithmic methods to exploit the above observations. In particular, the latter extends it to continuous parameters by considering the modified problem

$$x_{f_\gamma}^* = \arg \min_x f_\gamma(x); \quad (10)$$

where

$$f_\gamma(x) = -\log \left[G_\gamma * e^{-f(x)} \right] \quad (11)$$

with G_γ being the heat kernel, defined without the normalizing constant

$$G_\gamma(x) = e^{-\frac{\|x\|^2}{2\gamma}}.$$

They show that, under certain assumptions, the modified loss $f_\gamma(x)$ is smoother than the original loss function $f(x)$ and leads to improved generalization performance for deep networks.

Remark 2. The expression for local entropy (11) suggests that $\exp(-f_\gamma(x))$ is the solution of the heat equation for initial data $e^{-f(x)}$, i.e., if $u(x, t)$ satisfies

$$u_t = \frac{1}{2} \Delta u \quad (\text{HE})$$

with $u(x, 0) = e^{-f(x)}$ and the Laplacian is $\Delta(u) = \sum_{i=1}^n \frac{\partial^2}{\partial x_i^2} u$, the solution $u(x, t) = f_t(x)$ where now the parameter γ is identified with time.

3.1. PDE interpretation of local entropy. Remark 2 leads us to our first observation as described by the following lemma. It is an application of the Cole-Hopf transformation (Evans, 1998) which connects the solutions of the heat equation to those of the Hamilton-Jacobi equation.

Lemma 3. *Local entropy $f_\gamma(x)$ with $\gamma = t$ is the solution of the initial value problem for the viscous Hamilton-Jacobi equation*

$$\begin{aligned} u_t + \frac{1}{2} |\nabla u|^2 &= \frac{1}{2} \Delta u, \\ u(x, 0) &= f(x). \end{aligned} \quad (\text{viscous-HJ})$$

Proof. Define $u(x, t) = -\log v(x, t)$. From (11), $v(x, t)$ solves the heat equation $v_t = \frac{1}{2} \Delta v$ with initial data $v(x, 0) = \exp(-f(x))$. Computing the derivatives gives

$$\begin{aligned} v_t &= -v \frac{\partial}{\partial t} f_t(x), \\ \nabla v &= -v \nabla f_t(x), \\ \Delta v &= -v \Delta f_t(x) + v |\nabla f_t(x)|^2. \end{aligned}$$

Combining these expressions gives (viscous-HJ). ■

Remark 4 (The time scale t is the same as the width of the kernel γ). Note that Lemma 3 identifies the parameter γ with t , the time-scale of the evolution of the PDE. Indeed, running the (viscous-HJ) equation for a longer time with the initial data $f(x)$ results in a smoother solution; this is equivalent to convolving the original loss with a Gaussian kernel with a larger variance. In the sequel, we use both terms interchangeably: t when referring to the evolution time of a PDE, and γ elsewhere.

3.2. Gradient of local entropy by convolution. We now evaluate the gradient of $f_t(x)$, i.e., $\nabla u(x, t)$ in Lemma 3.

Lemma 5. *The gradient of local entropy is given by*

$$-\nabla f_t(x) = \frac{1}{t} \int_{\mathbb{R}^n} (x - y) \rho^\infty(y; x) dy \quad (12)$$

where $\rho^\infty(y; x)$ is a probability distribution given by

$$\rho^\infty(y; x) = Z(x)^{-1} \exp\left(-f(y) - \frac{\|x - y\|^2}{2t}\right) \quad (13)$$

and the normalizing constant is $Z(x) = \int_y \exp\left(-f(y) - \frac{\|x - y\|^2}{2t}\right) dy$.

Proof. Differentiating $e^{-f_t(x)}$ gives

$$\begin{aligned} -\nabla f_t(x) e^{-f_t(x)} &= -\nabla \left(G_t * e^{-f(x)} \right) \\ &= -\nabla_x \int G_t(x - y) e^{-f(y)} dy \\ &= \int \frac{x - y}{t} G_t(y - x) e^{-f(y)} dy, \end{aligned}$$

which gives (12). ■

Remark 6. An alternative formula for the gradient $\nabla f_t(x)$ is obtained by observing that

$$\begin{aligned}\nabla f_t(x) e^{f_t(x)} &= -\nabla_x \left(G_t * e^{-f(x)} \right) \\ &= -\nabla_x \int_y G_t(y) e^{-f(x-y)} dy \\ &= \int_y \nabla f(x-y) G_t(y) e^{-f(x-y)} dy \\ &\Rightarrow \nabla f_t(x) = \int_y \nabla f(x-y) \rho_2^\infty(dy; x).\end{aligned}\tag{14}$$

The probability measure here is $\rho_2^\infty(y; x) \propto \left(-\frac{\|y\|^2}{2t} - f(x-y) \right)$ and this version explicitly averages the gradient $\nabla f(x-y)$ in the neighborhood of x .

Remark 7. The authors in [Chaudhari et al. \(2016\)](#) use Langevin dynamics ([Welling and Teh, 2011](#)) to evaluate the gradient in (12). Langevin dynamics belong to a broader class of algorithms called Markov chain Monte Carlo (MCMC), which gives access to samples from high-dimensional and intractable probability distributions by performing a gradient descent on the unnormalized log-density ([Robert and Casella, 2013](#); [Neal, 2011](#)). As discussed in Sec. 2.3, the convergence of such dynamics to the distribution $\rho^\infty(y; x)$ is exponentially slow for non-convex energies $f(y) + \frac{1}{2t}\|x-y\|^2$. The parameter $t > 0$ which is the variance of the Gaussian smoothing kernel helps alleviate this and if

$$\nabla^2 f(x) + t^{-1} I \geq 0,$$

the function is convex and we have the exponential convergence given by (8). Sec. 6 further elaborates this point.

3.3. ESGD: algorithmic implementation. The stochastic gradient descent equation for local entropy is

$$dx(s) = -\nabla f_\gamma(x) ds.\tag{15}$$

Lemma 5 states that the gradient $\nabla f_\gamma(x)$ can be computed by an average over an invariant distribution as

$$\nabla f_\gamma(x) = -\gamma^{-1} \int_{\mathbb{R}^n} (x-y) \rho^\infty(y; x) dy.$$

The distribution $\rho^\infty(y; x)$ defined in (13) can be computed using the Langevin updates in Remark 7. This amounts to performing the update

$$dy(s) = -\left(\nabla f(y) + \frac{y-x}{2t} \right) ds + \sqrt{2} dW(s).$$

It is easy to show that the Fokker-Planck equation (FP) has $\rho^\infty(y; x)$ as the invariant distribution for the above dynamics.

4. STOCHASTIC CONTROL INTERPRETATION

Lemma 3 which connects local entropy $f_\gamma(x)$ to the viscous Hamiltonian-Jacobi equation allows us to interpret the gradient descent dynamics as an optimal control problem. This interpretation does not have immediate algorithmic implications, however it does allow us to prove a theorem which tells us that the expected value of a minimum is improved when we follow the local entropy dynamics rather than the stochastic gradient descent dynamics.

Controlled stochastic differential equation are generalizations of the case of SDEs discussed in Sec. 2.3. See ([Fleming and Soner, 2006](#); [Fleming and Rishel, 2012](#)). Consider following controlled SDE

$$\begin{aligned}dx(s) &= -h(x) ds - c_\alpha \alpha(s) ds + \sqrt{2\beta^{-1}} dW(s) \quad \text{for } t \leq s \leq T, \\ x(0) &= x.\end{aligned}\tag{CSGD}$$

Here c_α is a parameter which we will set later, and $h(x)$ will be either identically zero, or equal to $\nabla f(x)$. For fixed controls α , the generator for (CSGD) is given by

$$\mathcal{L}_\alpha := -\left[h + c_\alpha \alpha \right] \cdot \nabla + \beta^{-1} \Delta.$$

We now define a stochastic optimal control problem with a terminal cost $V : \mathbb{R}^n \rightarrow \mathbb{R}$. The expected cost over paths of (CSGD) for this problem is given by

$$\mathcal{C}(x(\cdot), \alpha(\cdot)) = \mathbb{E} \left[V(x(T)) + \frac{c_\alpha}{2} \int_0^T \|\alpha(s)\|^2 ds \right].\tag{16}$$

Let $u(x, t)$ be the minimum expected cost as a function of x and time t , it is achieved using the optimum over an admissible choice of controls, i.e.,

$$u(x, t) = \min_{\alpha(\cdot)} \mathcal{C}(x(\cdot), \alpha(\cdot)).$$

It can be shown that $u(x, t)$ is the unique viscosity solution of the Hamilton-Jacobi-Bellman (HJB) equation (Fleming and Soner, 2006; Fleming and Rishel, 2012), which leads to

$$\begin{aligned} u_t &= -h \cdot \nabla u - \frac{c_\alpha}{2} |\nabla u|^2 + \beta^{-1} \Delta u \quad \text{for } t \leq s \leq T, \\ u(x, t) &= V(x). \end{aligned} \tag{HJB}$$

along with

$$\alpha(x, t) = \nabla u(x, t) \tag{17}$$

Note that both SGD and gradient descent for local entropy are special cases of the dynamics governed by (HJB). For the first case, set $h(x) := \nabla f(x)$, $c_\alpha = 0$ and $V(x) = f(x)$. The (CSGD) dynamics becomes the original SGD dynamics

$$dx(s) = -\nabla f(x) ds + \beta^{-1} dW(s)$$

with the natural terminal cost, $\mathcal{C}(x(\cdot), \alpha(\cdot)) = \mathbb{E}[f(x(T))]$. Note that this is the “uncontrolled” case and as we expect, it minimizes the average loss over realizations of Wiener process. For the second case, set $c_\alpha = 1$, $\beta = 2$ and $h = 0$, so that (HJB) becomes

$$u_t = -\frac{1}{2} |\nabla u|^2 + \frac{1}{2} \Delta u \quad \text{for } t \leq s \leq T$$

with the initial condition $u(x, t) = f(x)$; this is equivalent to the (viscous-HJ) in Lemma 3. Controlled SGD is thus a way to interpolate between the dynamics of local entropy and the dynamics of SGD. In other words, local entropy $f_\gamma(x)$ is the solution of the (HJB) equation and the gradient of local entropy $\nabla u(x, t)$ can be interpreted as the optimal control $\alpha(x, t)$ where the cost is composed of two elements: one which minimizes the terminal loss, and a runtime cost which penalizes the control effort quadratically.

4.1. Improvement in the value function. The optimal control interpretation above allows us to provide the following theorem for the improvement in the value function obtained by local entropy as compared to stochastic gradient descent.

Theorem 8. *For a deterministic time $t \geq 0$ and any terminal loss $V(x)$, we have*

$$\mathbb{E}[V(x_{\text{csgd}}(t))] \leq \mathbb{E}[V(x_{\text{sgd}}(t))] - \frac{1}{2} \mathbb{E} \left[\int_0^t \|\alpha(x_{\text{csgd}}(s), s)\|^2 ds \right].$$

where $x_{\text{csgd}}(s)$ and $x_{\text{sgd}}(s)$ satisfy (CSGD) and (SGD), respectively, for the same initial data $x_{\text{csgd}}(0) = x_{\text{sgd}}(0) = x_0$, and $h(x) = \nabla f(x)$, $c_\alpha = 1$ and $\beta = 2$. The optimal control is $\alpha(s)$ and satisfies (17) where $u(x, t)$ is the solution of the (HJB) equation with initial data $u(x, 0) = V(x)$.

Proof. Let $v(x, t) = \mathbb{E}[V(x(t))]$, i.e., $v(x, t)$ is the solution of the PDE $v_t = \mathcal{L}v$, with a linear operator

$$\mathcal{L} = \nabla f(x) \cdot \nabla + \frac{1}{2} \Delta.$$

Similarly, let $u(x, t)$ be the solution of (HJB). Note that

$$u_t = \mathcal{L}u - \frac{c_\alpha}{2} |\nabla u|^2 \leq 0.$$

We now use the maximum principle (Evans, 1998) to get

$$u(x, t) \leq v(x, t), \quad \text{for all } t \geq 0; \tag{18}$$

since $u(x, 0) = v(x, 0) = V(x)$. Use the definition to get

$$v(x, t) = \mathbb{E}[V(x(t)) \mid x(0) = x_0];$$

the expectation is taken over the paths of (SGD). Similarly,

$$u(x, t) = \mathbb{E} \left[V(x(t)) + \frac{1}{2} \int_0^t \|\alpha\|^2 ds \right]$$

where $\alpha(\cdot)$ is the optimal control; the expectation is taken over the paths of (CSGD). Together, this gives the desired result. ■

Remark 9. Note that the second term on the right hand side in Theorem 8 above can also be written as

$$\frac{1}{2} \mathbb{E} \left[\int_0^t \|\nabla u(x_{\text{csgd}}(s), s)\|^2 ds \right].$$

The improvement of (CSGD) or local entropy over (SGD) is exactly the action of the kinetic energy in the dynamics over the optimal path.

4.2. Wider minima for controlled SGD. As discussed in Sec. 3, the width of minima that SGD converges to can be connected to generalization error of a deep network. The larger the width, the smaller is the difference between the performance of a classifier on the training set and an unknown validation set, which is desirable in machine learning. We can use the loss $f_\gamma(x)$ as a proxy for the width by expanding $f(y)$ around the minimum x^* . For small enough γ ,

$$\begin{aligned} f_\gamma(x^*) &= -\log \int_y \exp \left(-\frac{\|x^* - y\|^2}{2\gamma} - f(y) \right) dy \\ &\approx f(x^*) - \log \int_y \exp \left[-\frac{1}{2} (x^* - y)^\top \left(\nabla^2 f(x^*) + \gamma^{-1} I \right) (x^* - y) \right] dy \\ &= f(x^*) + \log \det \left(\nabla^2 f(x^*) + \frac{I}{\gamma} \right) + \text{constant} \\ &= \sum_{i=1}^n \lambda_i \left(\nabla^2 f(x^*) + \frac{1}{\gamma} \right), \end{aligned}$$

up to constants; here $\lambda_i(A)$ is the i^{th} eigenvalue of the matrix A . Note that since x^* is a minimum $\nabla f(x^*) = 0$ and $\nabla^2 f(x^*)$ is a positive semi-definite matrix. The smaller the eigenvalues λ_i , the smaller local entropy $f_\gamma(x^*)$ and wider the minimum. An application of Theorem 8 along with this result gives the following corollary.

Corollary 10. *If $V(x) = f_\gamma(x)$ in Theorem 8, in expectation, minima discovered by (CSGD) are wider than those discovered by (SGD). More precisely,*

$$\mathbb{E} [f_\gamma(x_{\text{csgd}}(t))] \leq \mathbb{E} [f_\gamma(x_{\text{sgd}}(t))] - \frac{1}{2} \mathbb{E} \left[\int_0^t \|\alpha(x_{\text{csgd}}(s), s)\|^2 ds \right].$$

where $t > 0$ is deterministic.

Proof. Consider a large enough t such that $\|x_{\text{csgd}}(t) - x_{f_\gamma}^*\| \leq \varepsilon$ and $\|x_{\text{sgd}}(t) - x_f^*\| \leq \varepsilon$ where $x_{f_\gamma}^*$ and x_f^* are local minima of $f_\gamma(x)$ and $f(x)$, respectively and $\varepsilon = \mathcal{O}(\gamma^{-1/2})$. We then have that $f_\gamma(x_{f_\gamma}^*) \leq \mathbb{E} [f_\gamma(x_{\text{csgd}}(t))]$ and $\mathbb{E} [f_\gamma(x_{\text{sgd}}(t))] \leq f_\gamma(x_f^*) + L_{f_\gamma} \varepsilon$ where L_{f_γ} is the Lipschitz constant of $f_\gamma(x)$. Combining these gives

$$f_\gamma(x_{f_\gamma}^*) \leq \mathbb{E} [f_\gamma(x_{f_\gamma}^*)] - \frac{1}{2} \mathbb{E} \left[\int_0^t \|\alpha(x_{\text{csgd}}(s), s)\|^2 ds \right] + \mathcal{O}(\gamma^{-1/2}).$$

■

5. HOPF-LAX FORMULA FOR THE HAMILTON-JACOBI EQUATION

In addition to the connection with (viscous-HJ) provided by Lemma 3, we can also explore the non-viscous Hamilton-Jacobi equation. This case with no viscosity is simpler to analyze, since the corresponding dynamics are deterministic and allow us to discuss minimizers instead of densities. In particular, we have a much simpler formula for the gradient of the solution, since there is no averaging against the invariant measure. In addition, semi-concavity of the solution follows directly from the Hopf-Lax formula. We consider the following initial value problem for the Hamilton-Jacobi equation in this section.

$$\begin{aligned} u_t + \frac{1}{2} |\nabla u|^2 &= 0 \\ u(x, 0) &= f(x). \end{aligned} \tag{HJ}$$

5.1. Hopf-Lax solution and dynamics for the gradient. The Hopf-Lax formula (Evans, 1998) gives the viscosity solution for this equation as

$$u(x, t) = \inf_y \left\{ f(y) + \frac{1}{2t} \|x - y\|^2 \right\}. \quad (\text{HL})$$

A function $f(x)$ is semi-concave with a constant C if $f(x) - \frac{C}{2} \|x\|^2$ is concave Cannarsa and Sinestrari (2004). Define $g(x; y) = f(y) + \frac{1}{2t} \|x - y\|^2$ to be a function of x parametrized by y . Each $g(x; y)$ is semi-concave with constant $1/t$ and hence $u(x, t)$, the infimum over such functions, is also semi-concave with the same constant, $1/t$. Semi-concavity of solutions with analogous bounds can be established for a more general class of equations, including (viscous-HJ) and (HJ) (cf. Sec. 7).

We now discuss how to obtain $\nabla_x u(x, t)$ using the Hopf-Lax formula.

Lemma 11. *Let $u(x, t)$ be given by (HL). If $\nabla_x u(x, t)$ exists, then it is given by*

$$\nabla_x u(x, t) = \frac{x - y^*}{t} = \nabla f(y^*), \quad (19)$$

where y^* is the optimizer in (HL). Moreover, suppose that

$$\nabla^2 f(x) + t^{-1} I \geq \lambda I$$

for some $\lambda > 0$. Then the gradient $p^* := \nabla_x u(x, t)$ is the unique steady solution of the dynamics

$$\frac{dp(s)}{ds} = -t \left(p(s) - \nabla f(x - t p(s)) \right). \quad (20)$$

Moreover, the convergence to p^* is exponential, i.e.,

$$\|p(s) - p^*\|_2 \leq \|p(0) - p^*\|_2 e^{-\lambda s t}.$$

Remark 12 (inf convolutions and the proximal operator). The solution of the HJ equation given by the Hopf-Lax formula (HL) is also called inf-convolution of the functions $f(x)$ and $\frac{1}{2t} \|x\|^2$ (Cannarsa and Sinestrari, 2004). This is closely related to the proximal operator (Moreau, 1965; Rockafellar, 1976) defined by

$$y^* := \text{prox}_{tf}(x) = \arg \min_y \left\{ f(y) + \frac{1}{2t} \|y - x\|^2 \right\}$$

Proof. The first equality is a direct application of Danskin's theorem (Bertsekas et al., 2003, Prop. 4.5.1). Let us rewrite (HL) with $ty' = x - y$ to obtain

$$u(x, t) = \inf_{y'} \left\{ f(x - ty') + \frac{t}{2} \|y'\|^2 \right\}.$$

Differentiating the above equation with respect to x (again by Danskin's theorem) gives

$$\nabla u(x, t) = \nabla f(x - ty'^*) = \nabla f(y^*).$$

Rewrite (HL) with $ty' = x - y$ to get

$$u(x, t) = \inf_{y'} \left\{ f(x - ty') + \frac{t}{2} \|y'\|^2 \right\} := \inf_{y'} g(y').$$

Note that (20) is the gradient descent dynamics on $g(y')$ with $p(s)$ identified by y' . Since $g(y)$ is (λt) -convex by assumption, we can obtain a contraction and exponential convergence to the minimizer p^* of this ordinary differential equation (ODE) (Santambrogio, 2015). ■

Remark 13. Note that the slow convergence of Langevin dynamics is not alleviated by the Hopf-Lax formula (HJ). While (19) is formally true, finding y^* algorithmically involves solving the minimization in (HL) which involves the same restriction for convexity.

5.2. HJ equation: algorithmic implementation. Let us compute a discretization for the ODE in (20) by setting

$$\frac{dp}{ds} = \frac{p^{s+1} - p^s}{ds} + \mathcal{O}(ds^2).$$

This leads to the iteration

$$p^{s+1} = (1 - t \, ds) p^s + t \, ds \, \nabla f(x - t p^s) \quad (21)$$

which is stable for $0 \leq ds \leq t^{-1}$ and converges globally under the convexity assumption of Lemma 11. Note that we can set $ds = t^{-1}$ to get the scheme

$$p^{s+1} = \nabla f(x - t p^s), \quad \text{with } p^1 = \nabla f(x). \quad (22)$$

This is actually equivalent to the method of characteristics for solving the non-viscous Hamilton-Jacobi equation (Evans, 1998) for small time. This equivalence is seen by identifying $y' = p$ as in the proof of Lemma 11. The fixed point in (19) given by

$$p^* = \nabla f(x - t p^*)$$

and can be solved by performing

$$p^{s+1} = \nabla f(x - t p^s). \quad (23)$$

This iteration is convergent if $I + t \nabla^2 f(x) > 0$.

5.3. Widening of minima by the Hamilton-Jacobi equation. As can be seen in Figure 1, solutions of the Hamilton-Jacobi have additional remarkable properties with respect to local minima. In particular, for small values of t (which depend on the derivatives of the initial function) local minima are preserved. To motivate these properties, consider a one-dimensional function $f(x)$ with $x \in \mathbb{R}$ in the Hopf-Lax formula for the non-viscous HJ equation (HJ). The fixed point of the iteration in (23) is

$$p = f'(x - p \, t)$$

where $p = u_x(x, t)$. The solutions of this equation remain classical until the characteristics intersect, i.e., until the smallest time, t^* such that $t^* f''(x - p t^*) + 1 = 0$.

Remark 14 (Widening of convex regions and contraction of concave regions). For a one-dimensional $f(x)$, we obtain the following remarkable feature for the HJ equation. Consider a smooth $f(x)$ which is convex between $x_0 \leq x \leq x_1$ and concave elsewhere; we require $f''(x_0) = f''(x_1) = 0$. We now have

$$\begin{aligned} p_x &= f''(x - t \, p) (1 - t \, p_x) \\ \Rightarrow p_x &= \frac{f''(x - t \, p)}{1 + t \, f''(x - t \, p)}. \end{aligned}$$

Thus $p_x > 0$ if $f''(x - t \, p) > 0$ and it is negative if $f''(x - t \, p) < 0$. Now pick a value of x such that $x - t \, p = x_1$ where $p = 0$; note that $x > x_1$. The critical point defined by $u_x = 0$ thus moves to the right of x_1 ; similarly the critical point x_0 moves to the left. Figure 1 shows an example of this phenomenon.

Remark 15. In the higher dimensional case, well-known properties of the inf-convolution can be used to establish the following facts. If $f(x)$ is convex, $u(x, t)$ given by (HL) is also convex; thus, any minimizer of f also minimizes $u(x, t)$. Moreover, for bounded $f(x)$, using the fact that $\|y^*(x) - x\| = \mathcal{O}(\sqrt{t})$, one can obtain a local version of the same result, viz., for short times t , a local minimum persists. Similar to the example in Fig. 1, local minima vanish in the solution for longer times.

Widening of the loss around local minima by the Hamilton-Jacobi equation can also be described by “semiconcavity” which expresses the fact that the maximal values of a second derivative $u_{x_i x_i}$ are decreasing in time. These estimates are shared by a whole class of equations, as discussed in Cannarsa and Sinestrari (2004) and Sec 7 below.

6. DERIVATION OF LOCAL ENTROPY VIA HOMOGENIZATION OF SDES

This section introduces the technique of homogenization for stochastic differential equations and gives a mathematical treatment to the result of Lemma 5 which was missing in Chaudhari et al. (2016). In addition to this, homogenization allows us to rigorously show that an algorithm called Elastic-SGD (Zhang et al., 2015) that was heuristically connected to a distributed version of local entropy in Baldassi et al. (2016a) is indeed equivalent to local entropy.

Homogenization is a technique used to analyze dynamical systems with multiple time-scales that have a few fast variables that may be coupled with other variables which evolve slowly. Effectively, by computing ergodic averages over

the fast variables, we can reason about the evolution of the slow variables. Please refer to [Pavliotis and Stuart \(2008, Chap. 10, 17\)](#) for a detailed introduction. Consider the system of SDEs given by

$$\begin{aligned} dx(s) &= h(x, y) ds \\ dy(s) &= \frac{1}{\varepsilon} g(x, y) ds + \frac{1}{\sqrt{\varepsilon}} dW(s); \end{aligned} \quad (24)$$

where h, g are sufficiently smooth functions, $W(s) \in \mathbb{R}^n$ is the standard Wiener process and $\varepsilon > 0$ is the homogenization parameter which introduces a fast time-scale for the dynamics of $y(s)$. Let us define the generator for the second equation to be

$$\mathcal{L}_0 = g(x, y) \cdot \nabla_y + \frac{1}{2} \Delta_y.$$

We assume that for each fixed x , the fast-dynamics, $y(s)$, has a unique invariant probability measure denoted by $\rho^\infty(y; x)$ and the operator \mathcal{L}_0 has a one-dimensional null-space characterized by

$$\mathcal{L}_0 1(y) = 0, \quad \mathcal{L}_0^* \rho^\infty(y; x) = 0;$$

here $1(y)$ are all constant functions in y and \mathcal{L}_0^* is the adjoint of \mathcal{L}_0 . One can then show that for $\varepsilon \mathcal{L} 1$, and for times of $\mathcal{O}(1)$, the dynamics in (24) can be approximated by

$$d\bar{x}(s) = \bar{h}(x) ds$$

where the homogenized vector field for x is defined as

$$\bar{h}(x) = \int h(x, y) \rho^\infty(dy; x).$$

The variable $y(s)$ is simply distributed as $\rho^\infty(y; x(s))$. We can also obtain bounds on the approximation error, in particular,

$$\mathbb{E} \left[\sup_{0 \leq s \leq T} \|x(s) - \bar{x}(s)\|^p \right] \leq C \varepsilon^{p/2}$$

for some constant $C > 0$ and all $p > 1$. Moreover, by ergodicity, we can compute

$$\bar{h}(x) = \int h(x, y) \rho^\infty(dy; x) = \lim_{T \rightarrow \infty} \frac{1}{T} \int_0^T h(x, y(s)) ds$$

independent of the initial value $y(0)$.

6.1. Derivation of local entropy via homogenization of SDEs. We can write a continuous-time differential equation for the optimization in Prob. (3) as

$$dx(s) = -\nabla f_\gamma(x) ds.$$

Lemma 5 and Remark 7 state that $\nabla f_\gamma(x)$ can be computed by an average

$$\nabla f_\gamma(x) = -\gamma^{-1} \int_{\mathbb{R}^n} (x - y) \rho^\infty(y; x) dy.$$

Hence, let us consider the following system of SDEs as a model for Prob. (3).

$$\begin{aligned} dx(s) &= -\gamma^{-1} (x - y) ds \\ dy(s) &= -\frac{1}{\varepsilon} \left[\nabla f(y) + \frac{1}{\gamma} (y - x) \right] ds + \frac{1}{\sqrt{\varepsilon}} dW(s). \end{aligned} \quad (\text{ESGD})$$

Note that the Fokker-Planck equation for the density of $y(s)$ is given by

$$\rho_t = \mathcal{L}_0^* \rho = \nabla_y \cdot (\nabla_y H \rho) + \frac{1}{2} \Delta_y \rho; \quad (25)$$

where $H(x, y; \gamma) = f(y) + \frac{1}{2\gamma} \|x - y\|^2$. The invariant measure for this Fokker-Planck equation is thus

$$\rho^\infty(y; x) \propto \exp(-H(x, y; \gamma)/\varepsilon)$$

which agrees with (13) in Lemma 5 for $\varepsilon = 1$.

Theorem 16. As $\varepsilon \rightarrow 0$, the system (ESGD) converges to the homogenized dynamics given by

$$d\bar{x}(s) = -\nabla f_\gamma(x) ds.$$

Moreover, $\nabla f_\gamma(x) = -\gamma^{-1} (\bar{x} - \langle y \rangle)$ where

$$\langle y \rangle = \int y \rho^\infty(dy; \bar{x}) = \lim_{T \rightarrow \infty} \int_0^T y(s) ds \quad (26)$$

where $y(s)$ is the solution of (ESGD) with x fixed.

Proof. The result follows immediately from the convergence result in Sec. 6 for the system (24). The homogenized vector field is

$$\bar{h}(x) = -\gamma^{-1} \int (x - y) \rho^\infty(dy; x)$$

which is equivalent to $\nabla f_\gamma(x)$ from Lemma 5. ■

Remark 17. Theorem 16 relies upon the existence of an ergodic, invariant measure $\rho^\infty(dy; x)$. As we discussed in Sec. 4, convergence to such a measure is fast only if the underlying energy, $H(x, y; \gamma)$, is convex in y ; in our case, this happens if $\nabla^2 f(x) + \gamma^{-1} I \geq 0$ at all x . Note that for large γ , the invariant measure of $y(s)$ is still $\propto \exp(-f(x))$ but because $f(x)$ is a non-convex function, convergence to its Gibbs distribution does not happen at $\mathcal{O}(1)$ time scales. It is an important question for future work to understand the dynamics of (ESGD) for large γ and in general, characterize the transient behavior of the Fokker-Planck equation (25) for non-convex losses.

6.2. H-ESGD: algorithmic implementation. Theorem 16 shows that the homogenized dynamics converge to the correct gradient of local entropy as given by Lemma 5. The ESGD algorithm of Sec. 3.3 can therefore be implemented in a different way now, viz., by solving the system of equations in (ESGD) for a non-zero ε . We perform an Euler discretization of the system of equations in (ESGD) to get the update rule

$$\begin{aligned} x^{k+1} &= \begin{cases} -\eta \gamma^{-1} (x^k - y^k) & \text{if } (\varepsilon k) \text{ is an integer,} \\ x^k & \text{else.} \end{cases} \\ y^{k+1} &= -\left[\nabla f(y^k) + \gamma^{-1} (y^k - x^k) \right]. \end{aligned} \quad (\text{H-ESGD})$$

Note that the gradient $f(y^k)$ in a deep network is evaluated over a mini-batch and is already noisy which is why the Wiener process term in (ESGD) is absent. The parameter η is the step-size of the x update. In practice, we typically set $\varepsilon = 1/20$.

6.3. Heat equation versus the viscous Hamilton-Jacobi equation. Lemma 3 showed that local entropy is the solution to the viscous Hamilton-Jacobi equation (viscous-HJ). The homogenization dynamics in (ESGD) can thus be interpreted as a way of smoothing of the original loss $f(x)$ to aid optimization. Other partial differential equations could also be used to achieve a similar effect. For instance, let us consider the following dynamics for the heat equation:

$$\begin{aligned} dx(s) &= -\nabla f(x - y) ds \\ dy(s) &= -\frac{1}{\varepsilon} y ds + \frac{1}{\sqrt{\varepsilon}} dW(s). \end{aligned} \quad (\text{HEAT})$$

Using a very similar analysis as above, we can see that the invariant distribution for this system is $\rho^\infty(dy; x) = G_\gamma(y)$. In other words, the fast-dynamics for y is decoupled from x and $y(s)$ converges to a Gaussian distribution with mean zero and variance γI . The homogenized dynamics is given by

$$d\bar{x}(s) = -\left(\nabla f(x) \right) * G_\gamma ds$$

which leads to a local averaging of the gradients. To contrast this with local entropy, note that we can rewrite the system (ESGD) as

$$\begin{aligned} dx(s) &= -\nabla f(x - y) ds \\ dy(s) &= -\frac{1}{\varepsilon} \left[\frac{y}{\gamma} - \nabla f(x - y) \right] ds + \frac{1}{\sqrt{\varepsilon}} dW(s), \end{aligned} \quad (\text{ESGD-2})$$

using Remark 6 and (14). The extra term in the $y(s)$ dynamics with respect to (HEAT) is exactly the distinction between the smoothing performed by local entropy and the smoothing performed by heat equation. The latter is common in the deep learning literature under different forms, e.g., Gulcehre et al. (2016) and Mobahi (2016). The former version however

has much better empirical performance (cf. experiments in Sec. 8 and Chaudhari et al. (2016)) as well as improved convergence in theory (cf. Theorem 8). Moreover, at a local minimum, (HEAT) is equivalent to local entropy (ESGD-2).

6.3.1. Estimate of ρ^∞ for a quadratic $f(x)$. Local entropy computes a non-linear average of the gradient in the neighborhood of x by weighing the gradients according to the steady state measure $\rho^\infty(y; x)$ (cf. Lemma 5). In this section, we show that using a quadratic approximation of $f(x)$, say, by an approximation of the Hessian $\nabla^2 f(x)$, we can compute the gradient $\nabla f_\gamma(x)$ cheaply. The invariant measure $\rho^\infty(y; x)$ is a Gaussian distribution in this case and the gradient $f_\gamma(x)$ can thus be evaluated by a sample average of $\nabla f(x + \eta)$ where η is sampled from this distribution.

Lemma 18. *If $f(x)$ is quadratic, if $p = \nabla f(x)$ and $Q = \nabla^2 f(x)$, the invariant measure $\rho^\infty(y; x)$ of (13) is a normal distribution with mean μ and covariance Σ given by*

$$\mu = x - \Sigma p \quad \text{and} \quad \Sigma = (Q + \gamma I)^{-1}.$$

In particular, for $\gamma > \|Q\|_2$, we have

$$\mu = x - (\gamma^{-1} I - \gamma^{-2} Q) p \quad \text{and} \quad \Sigma = \gamma^{-1} I - \gamma^{-2} Q.$$

Proof. Without loss of generality, a quadratic $f(x)$ centered at $x = 0$ can be written as

$$\begin{aligned} f(x) &= f(0) + p^\top x + \frac{1}{2} x^\top Q x, \\ \Rightarrow f(x) + \frac{\gamma}{2} x^2 &= f(0) - \mu^\top p + \frac{1}{2} (y - \mu)^\top (Q + \gamma I) (y - \mu) \end{aligned}$$

by completing the square. The distribution $\exp(-f(y) - \frac{\gamma}{2} y^2)$ is thus a normal distribution with mean $\mu = x - \Sigma p$ and variance $\Sigma = (Q + \gamma I)^{-1}$ and an appropriate normalization constant. The approximation $\Sigma = \gamma^{-1} I - \gamma^{-2} Q$ which avoids inverting the Hessian follows from the Newman series for the matrix inverse; it converges for $\gamma > \|Q\|_2$ and is accurate up to $\mathcal{O}(\gamma^{-3})$. \blacksquare

Remark 19. The result in Lemma 18 is straightforward, yet illustrative. While the heat equation performs a local averaging around x , up to a quadratic approximation of $f(x)$, local entropy averages the gradient after one step of gradient descent, i.e., at $x - \Sigma \nabla f(x)$. As we showed in Theorem 8, this leads to faster convergence.

6.4. Elastic-SGD as local entropy. Elastic-SGD is an algorithm introduced by Zhang et al. (2015) for distributed training of deep neural networks and aims to minimize the communication overhead between a set of workers that together optimize replicated copies of the original function $f(x)$. For $p > 0$ distinct workers, they solve the problem

$$\min_{x_1, \dots, x_p} \sum_{i=1}^p f(x_i) + \frac{1}{2\gamma} \|x_i - p^{-1} \sum_{j=1}^p x_j\|^2. \quad (27)$$

The formulation in (27) lends itself easily to a distributed optimization where worker i performs the following update independently

$$x_i^{s+1} = x_i^s - \eta_s \left[\nabla f(x_i) + \frac{1-p^{-1}}{\gamma} \left(x_i - p^{-1} \sum_{j=1}^p x_j \right) \right];$$

while communicating the average $p^{-1} \sum_{j=1}^p x_j$ amongst all workers. This algorithm was later shown to be connected to the local entropy loss $f_\gamma(x)$ by Baldassi et al. (2016a) using arguments from replica theory. We can use homogenization to show that the dynamics of the workers optimizes exactly $f_\gamma(x)$. Consider the system of equations

$$\begin{aligned} dx(s) &= \frac{p^{-1}}{\gamma} \sum_{i=1}^p (x - y_i) ds \\ dy_i(s) &= -\frac{1}{\varepsilon} \left[\nabla f(y_i) + \frac{1}{\gamma} (y_i - x) \right] ds + \frac{1}{\sqrt{\varepsilon}} dW_i(s); \quad \text{for } 1 \leq i \leq p. \end{aligned} \quad (\text{Elastic-SGD})$$

We construct an auxiliary variable y that is the concatenation of all variables y_i . Similar to Sec. 6.1, define the Hamiltonian to be $H(x, y; g) = \sum_{i=1}^p f(y_i) + \frac{1}{2\gamma} \|x - p^{-1} \sum_{i=1}^p y_i\|^2$. The invariant measure for the $y(s)$ dynamics is the product measure of the y_i s,

$$\rho^\infty(y; x) \propto \exp\left(-H(x, y; g)/\varepsilon\right),$$

while the homogenized vector field for x is

$$\bar{h}(x) = \frac{1}{\gamma} (x - \langle y \rangle)$$

where $\langle y \rangle = p^{-1} \int \sum_{i=1}^p y_i \rho^\infty(dy; x)$. Under ergodicity, we can replace the average over the invariant measure using the temporal average, i.e.,

$$\begin{aligned} \langle y \rangle &= \lim_{T \rightarrow \infty} (Tp)^{-1} \sum_{i=1}^p \int_0^T y_i(s) ds \\ &= \lim_{T \rightarrow \infty} \int_0^T y_1(s) ds. \end{aligned} \quad (28)$$

The second equality again follows by ergodicity, the invariant distribution of $y_1(s)$ is the same as that of any of the other workers $y_i(s)$. The algorithm as implemented in [Zhang et al. \(2015\)](#) uses $T = 1$ and $p = 8$ or $p = 16$ in (28). In our experiments, we typically use $T = 5$ or $T = 20$ using the ergodic form (26) which is the same as the second equality.

6.5. Forward-backward equation and mean-field games. We wrote (HJB) as an equation in forward time. However, we can also relabel time and write a backward-time equation using dynamic programming. The density $\rho(x, t)$ still evolves in forward-time using the Fokker-Planck equation with the important difference that the potential $u(x, t)$ that defines the flow of the density through its gradient now evolves in backwards. We can write this forward-backward system as

$$\begin{aligned} -u_t &= -h \cdot \nabla u - \frac{c\alpha}{2} |\nabla u|^2 + \beta^{-1} \Delta u \\ \rho_t &= -\nabla \cdot (\nabla u \rho) + \Delta \rho, \end{aligned} \quad (29)$$

for $0 \leq s \leq T$ along with the terminal and the initial data

$$\begin{aligned} u(x, T) &= V(x), \\ \rho(x, 0) &= \rho_0(x). \end{aligned}$$

This system is an uncoupled mean field game ([Lasry and Lions, 2007](#); [Huang et al., 2006](#)). Mean field games are a generalization of stochastic control problem which allows for a coupling between the density evolution and the stochastic optimal control problem. In particular, this suggests that the system (Elastic-SGD) can be interpreted as an uncoupled mean field game and it may be possible to introduce a different coupling than the bias towards the mean amongst the workers in the distributed setting. Let us note that this mean-field game interpretation can then be used to prove an analogue of Theorem 8 and obtain an estimate of the improvement in the terminal reward.

7. REGULARIZATION AND SEMI-CONCAVITY

The PDE approaches discussed in Sec. 3, and local entropy in particular, result in a smoother loss function. Indeed, the latter involves a convolution of $e^{-f(x)}$ by a Gaussian. In this section, we establish that the modified optimization problem 10 has a smoother loss $f_\gamma(x)$. Instead of directly analyzing $f_\gamma(x)$, we exploit the fact that it is the solution of the viscous HJ equation which allows us to use standard semi-concavity estimates from PDE theory ([Evans, 1998](#); [Cannarsa and Sinestrari, 2004](#)) and quantify the amount of smoothing. Note that these estimates do not depend on the coefficient of viscosity, β , so they apply to the HJ equation as well.

7.1. Bounds on the Hessian. We had a basic semi-concavity estimate on the solution of the non-viscous (HJ) equation in Sec. 5.1. Let us look at a basic example. The solution of the (viscous-HJ) equation with $u(x, 0) = \|x\|^2/2$ is

$$u(x, t) = \frac{\|x\|^2}{2(t+1)} + \log(t+1).$$

In other words, the viscous HJ equation widens the parabola $\|x\|^2/2$ with time t . Note that t is the variance of the heat kernel used in the definition of local entropy (11). As $t \rightarrow \infty$, the curvature of $u(x, t)$ goes to zero.

Lemma 20. *Suppose $u(x, t)$ is the solution of (viscous-HJ). If*

$$C_k = \sup_x u_{x_k x_k}(x, 0) \quad \text{and} \quad C_{\text{Lap}} = \sup_x \Delta u(x, 0),$$

then

$$\sup_x u_{x_k x_k}(x, t) \leq \frac{1}{C_k^{-1} + t}$$

and

$$\sup_x \Delta u(x, t) \leq \frac{1}{C_{\text{Lap}}^{-1} + t/n}.$$

Proof. Let $w = u_{x_k x_k}$, differentiating (viscous-HJ) twice gives

$$w_t + \nabla u \cdot \nabla w + \sum_{i=1}^n u_{x_i x_k}^2 = \frac{1}{2} \Delta w. \quad (30)$$

Using $u_{x_k x_k}^2 = w^2$, we have

$$w_t + \nabla u \cdot \nabla w + w^2 - \frac{1}{2} \Delta w \leq 0.$$

Note that $w(x, 0) \leq C_k$ and the function

$$w'(x, t) = \frac{1}{C_k^{-1} + t}$$

is a spatially independent super-solution of the preceding equation with $w(x, 0) \leq w'(x, 0)$. By the comparison principle applied to w and w' , we have

$$w(x, t) = u_{x_k x_k}(x, t) \leq \frac{1}{C_k^{-1} + t}$$

for all x and $t \geq 0$, which gives the first result.

Now set $v = \Delta u$ and sum (30) over all k to obtain

$$\begin{aligned} v_t + \nabla u \cdot \nabla v + \sum_{i,j=1}^n u_{x_i x_j}^2 &= \frac{1}{2} \Delta v \\ \Rightarrow v_t + \nabla u \cdot \nabla v &\leq -\frac{1}{n} w^2 + \frac{1}{2} \Delta v \end{aligned}$$

by the Cauchy-Schwartz inequality. Now apply the comparison principle to $v'(x, t) = (C_{\text{Lap}}^{-1} + t/n)^{-1}$ to obtain the second result. \blacksquare

Remark 21 (Semiconcavity estimates). The advantage of the semiconcavity estimates is that even for very short time, we get a very large improvement in the (one-sided) bound on second derivatives. By contrast, the heat equation also smoothes, but the rate can be comparatively slow for short times. E.g., for $u_t = \Delta u$ and $u(x, 0) = f(x)$, the solution is $u(x, t) = \sum_{k=0}^{\infty} d_k e^{-\lambda_k t} \omega_k$ where $f(x) = \sum_{k=0}^{\infty} d_k \omega_k$ and λ_k are the corresponding eigenvalues.

7.1.1. Harmonic mean. Our semi-concavity estimates in Sec. 7.1 gave bounds on $\sup_x u_{x_k x_k}(x, t)$ and the Laplacian $\sup_x \Delta u(x, t)$. In this section, we extend the above estimates to characterize the eigenvalue spectrum more precisely. Our approach is motivated by experimental evidence in Chaudhari et al. (2016, Figure 1) and Sagun et al. (2016). The authors found that the Hessian of a typical deep network at a local minimum discovered by SGD has a very large proportion of its eigenvalues that are close to zero. This trend was observed for a variety of neural network architectures, datasets and dimensionality.

For such a Hessian, instead of bounding the largest eigenvalue or the trace (which is also the Laplacian), we obtain estimates of the harmonic mean of the eigenvalues. This effectively discounts large eigenvalues and we get an improved estimate of the ones close to zero, that dictate the width of a minimum. The harmonic mean of a vector $x \in \mathbb{R}^n$ is

$$\text{HM}(x) = \left(\frac{1}{n} \sum_{i=1}^n \frac{1}{x_i} \right)^{-1}.$$

The harmonic mean is more sensitive to small values as seen by

$$\min_i x_i \leq \text{HM}(x) \leq n \min_i x_i.$$

which does not hold for the arithmetic mean. To give an example, the eigenspectrum of a typical network (Chaudhari et al., 2016, Figure 1) has an arithmetic mean of 0.0029 while its harmonic mean is $\approx 10^{-10}$ which better reflects the large proportion of almost-zero eigenvalues.

Lemma 22. If Λ is the vector of eigenvalues of the symmetric positive definite matrix $A \in \mathbb{R}^{n \times n}$ and $D = (a_{11}, \dots, a_{nn})$ is its diagonal vector,

$$\text{HM}(\Lambda) \leq \text{HM}(D).$$

Proof. Majorization is a partial order on vectors with non-negative components (Marshall et al., 1979, Chap. 3) and for two vectors $x, y \in \mathbb{R}^n$, we say that x is majorized by y and write $x \preceq y$ if $x = Sy$ for some doubly stochastic matrix S . The diagonal of a symmetric, positive semi-definite matrix is majorized by the vector of its eigenvalues (Schur, 1923). For any Schur-concave function $f(x)$, if $x \preceq y$ we have

$$f(y) \leq f(x)$$

from Marshall et al. (1979, Chap. 9). The harmonic mean is also a Schur-concave function which can be checked using the Schur-Ostrowski criterion

$$(x_i - x_j) \left(\frac{\partial \text{HM}}{\partial x_i} - \frac{\partial \text{HM}}{\partial x_j} \right) \leq 0 \quad \text{for all } x \in \mathbb{R}_+^n$$

and we therefore have

$$\text{HM}(\Lambda) \leq \text{HM}(D).$$

■

Lemma 23. *If $u(x, t)$ is a solution of (viscous-HJ) and $C \in \mathbb{R}^n$ is such that $\sup_x u_{x_k x_k}(x, t) \leq C_k$ for all $k \leq n$, for a local minimum x^* of $u(x, t)$, we have*

$$\text{HM}(\Lambda) \leq \frac{1}{t + \text{HM}(C)^{-1}}$$

where Λ is the vector of eigenvalues of $\nabla^2 u(x^*, t)$.

Proof. For a local minimum x^* , we have $\text{HM}(L) \leq \text{HM}(D)$ from the previous lemma; here D is the diagonal of the Hessian $\nabla^2 u(x_{\min}, t)$. From Lemma 20 we have

$$u_{x_k x_k}(x^*, t) \leq C_k(t) = \frac{1}{t + C_k^{-1}}.$$

The result follows by observing

$$\text{HM}(C(t)) = \frac{n}{\sum_{i=1}^n C_k(t)^{-1}} = \frac{1}{t + \text{HM}(C)^{-1}}.$$

■

8. EMPIRICAL VALIDATION

We now discuss experimental results on deep neural networks that demonstrate that the PDE methods considered in this article achieve good regularization, aid optimization and lead to improved classification on modern datasets.

8.1. Setup for deep networks. In machine learning, one typically splits the data into three sets: (i) the training set D , used to compute the optimization objective (empirical loss f), (ii) the validation set, used to tune parameters of the optimization process which are not a part of the function f , e.g., mini-batch size, step-size, number of iterations etc., and, (iii) a test set, used to quantify generalization as measured by the empirical loss on previously-unseen (sequestered) data. However, for the benchmark datasets considered here, it is customary in the literature to not use a separate test set. Instead, one typically reports test error on the validation set itself; for the sake of enabling direct comparison of numerical values, we follow the same practice here.

We use two standard computer vision datasets for the task of image classification in our experiments. The MNIST dataset (LeCun et al., 1998) contains 70,000 gray-scale images of size 28×28 , each image portraying a hand-written digit between 0 to 9. This dataset is split into 60,000 training images and 10,000 images in the validation set. The CIFAR-10 dataset (Krizhevsky, 2009) contains 60,000 RGB images of size 32×32 of 10 objects (aeroplane, automobile, bird, cat, deer, dog, frog, horse, ship and truck). The images are split as 50,000 training images and 10,000 validation images. Figure 2 and Figure 3 show a few example images from these datasets.



FIGURE 2. MNIST

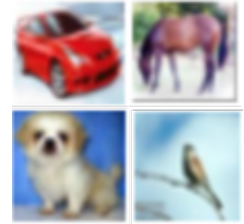


FIGURE 3. CIFAR-10

8.1.1. *Pre-processing.* We do not perform any pre-processing for the MNIST dataset. For CIFAR-10, we perform a global contrast normalization (Coates et al., 2010) followed by a ZCA whitening transform (sometimes also called the “Mahalanobis transformation”) (Krizhevsky, 2009). We use ZCA as opposed to principal component analysis (PCA) for data whitening because the former preserves visual characteristics of natural images unlike the latter, which better suits convolutional neural networks. We do not perform any data augmentation, i.e., transformation of input images by mirror-flips or translations, for MNIST and CIFAR-10.

8.1.2. *Loss function.* We defined the zero-one loss $f_i(x)$ for a deep network in Sec. 2.1. For classification tasks with K classes, it is common practice to construct a network with K distinct outputs. The output $y(x; \xi^i)$ is thus a vector of length K that is further normalized to sum up to 1 using the softmax operation defined in Sec. 8.2. The cross-entropy loss used for optimization is defined to be:

$$f_i(x) := - \sum_{k=1}^K \mathbf{1}_{\{y^i=k\}} \log y(x; \xi^i)_k.$$

We use the cross-entropy loss for all our experiments.

8.1.3. *Training procedure.* We run the following algorithms for each neural network:

- **ESGD:** the Entropy-SGD algorithm of Chaudhari et al. (2016) as described in Sec. 3.3,
- **HEAT:** smoothing by the heat equation by discretizing (HEAT),
- **H-ESGD:** homogenization implementation of Entropy-SGD given by (ESGD) in Sec. 6.2,
- **HJ:** fixed-point iteration of the Cole-Hopf formula for the Hamilton-Jacobi equation given by (23) in Sec. 5.2,
- **SGD:** stochastic gradient descent given by (4),

All the above algorithms are stochastic in nature; in particular, they sample a mini-batch of images randomly from the training set at each iteration before computing the gradient. We therefore report (and plot) the mean and standard deviation across 6 distinct random seeds for each experiment. The mini-batch size ($|i_t|$ in (4)) is fixed at 128. An “epoch” is defined to be one pass over the entire dataset, e.g., it consists of $\lceil 60,000/128 \rceil = 469$ iterations of (4) for MNIST with each mini-batch consisting of 128 different images. We use Nesterov’s momentum (Nesterov, 1983) set to 0.9 for all experiments and perform step-size annealing (cf. Sec. 2.4), i.e., reduce the step-size by a factor of 10 when the validation error remains constant over a few iterations.

We use SGD as a baseline for comparing the performance of the above algorithms in all our experiments.

Remark 24 (Number of gradient evaluations). A deep network evaluates the average gradient over an entire mini-batch of 128 images in one single back-propagation operation (Rumelhart et al., 1988). We define the number of back-props per weight by L . Note that SGD uses one back-prop per update ($L = 1$) while we use $L = 1/\varepsilon = 20$ back-props per update for (ESGD) and (H-ESGD). We perform $L = 5$ iterations to estimate the fixed point in HJ. For each of the algorithms above, we plot the training loss or the validation error against the number of “effective epochs”, i.e., the number of epochs multiplied by L which gives us a uniform scale to measure the computational complexity of various algorithms. This is a direct measure of the wall-clock time and is agnostic to the underlying hardware and software implementation.

Remark 25 (Tuning γ). Theorem 8 suggests that running the PDE for a longer time t (equivalently, for a longer γ , cf. Lemma 3) leads to an improvement in the value function. Related to this, Figure 1 shows that a large t leads to a smoother loss. We exploit this using a technique called “scoping” where we set γ to a large value and reduce it as training progresses. This reduces the smoothing effect and as $\gamma \rightarrow 0$, we have $\|f_\gamma(x) - f(x)\| \rightarrow 0$; this follows from the Hopf-Lax formula (HL). We set $\gamma = \gamma_0 (1 - \gamma_1)^k$ where k is the number of training iterations and tune γ_0 and γ_1 manually for all experiments so as to obtain the best validation error.

8.2. MNIST.

8.2.1. *Fully-connected network.* Consider a “fully-connected” network on MNIST

$$\text{mnistfc} : \text{input}_{784} \rightarrow \text{drop}_{0.2} \rightarrow \underbrace{\text{fc}_{1024} \rightarrow \text{drop}_{0.2}}_{\times 2} \rightarrow \text{fc}_{10} \rightarrow \text{softmax}.$$

The input layer reshapes each MNIST image as a vector of size 784. The notation fc_d denotes a dense matrix x^k in (1) with d output dimensions, followed by the ReLU nonlinearity (cf. Sec. 2.1) and an operation known as batch normalization (Ioffe and Szegedy, 2015) which whitens the output of the linear layer by subtracting the mean across a mini-batch and dividing by the standard deviation. The notation drop_p denotes the dropout layer (Srivastava et al., 2014) which

randomly sets a fraction p of the neurons to zero at each iteration. For 10 classes in the classification problem, we create an output vector of length 10 in the last fc layer followed by softmax which picks the largest element of this vector, which is interpreted as the output (or “prediction”) by this network. We use the standard cross-entropy loss for penalizing incorrect predictions for all networks considered in this article. The mnistfc network has $n = 1.86$ million parameters.

As Figure 4a and Table 1 show, the final validation error for all algorithms is quite similar. The convergence rate varies across them, in particular, ESGD converges fastest in this case. Note that mnistfc is a small network and the difference in the performance of the above algorithms, e.g., 1.08 % for ESGD versus 1.17 % for HJ, is minor.

8.2.2. *LeNet*. Our second network for MNIST is a convolutional neural network (CNN) denoted as follows:

LeNet : $\text{input}_{28 \times 28} \rightarrow \text{conv}_{20,5,3} \rightarrow \text{drop}_{0.25} \rightarrow \text{conv}_{50,5,2} \rightarrow \text{drop}_{0.25} \rightarrow \text{fc}_{500} \rightarrow \text{drop}_{0.25} \rightarrow \text{fc}_{10} \rightarrow \text{softmax}$.

The notation $\text{conv}_{c,k,m}$ denotes a 2D convolutional layer with c output channels, each of which is the sum of a channel-wise convolution operation on the input using a learnable kernel of size $k \times k$. It further adds ReLU nonlinearity, batch normalization and an operation known as max-pooling which down-samples the image by picking the maximum over a patch of size $m \times m$. Convolutional networks typically perform much better for image classification with fewer parameters; the LeNet network has only $n = 131,220$ parameters.

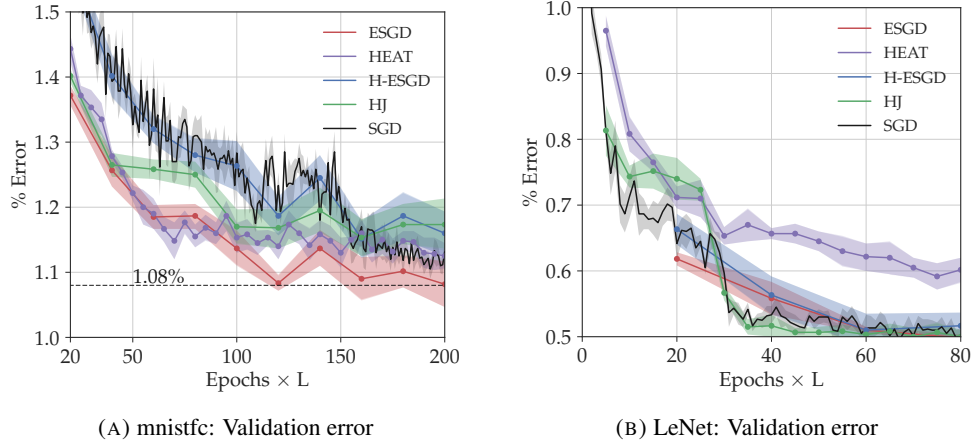


FIGURE 4. mnistfc and LeNet on MNIST (best seen in color)

The results for LeNet are described in Figure 4b and Table 1. This is a convolutional neural network and performs better than mnistfc on the same dataset. The final validation error is very similar for all algorithms at 0.50 % with the exception of the heat equation which only reaches 0.59 %. We can also see that the other algorithms converge quickly, in about half the number of effective epochs as that of mnistfc.

8.3. **CIFAR**. The CIFAR-10 dataset is more complex than MNIST and fully-connected networks typically perform poorly. We will hence employ a convolutional network for this dataset. We use the All-CNN-C network introduced by [Springenberg et al. \(2014\)](#) with a slight modification, viz., we add batch-normalization. In our notation, this is

All-CNN : $\text{input}_{3 \times 32 \times 32} \rightarrow \text{drop}_{0.2} \rightarrow \text{block}_{96,3} \rightarrow \text{block}_{192,3} \rightarrow \underbrace{\text{conv}_{192,3}}_{\times 2} \rightarrow \text{conv}_{10} \rightarrow \text{mean-pool}_{10} \rightarrow \text{softmax}$.

where

$\text{block}_{d,3} : \text{conv}_{d,3,1} \rightarrow \text{conv}_{d,3,1} \rightarrow \text{conv}_{d,3,1}^* \rightarrow \text{drop}_{0.5}$.

The final convolutional layer in above block denoted by conv^* is different from others; while they perform convolution at every pixel (“stride 1”), conv^* uses stride 2, thus downsampling by a factor of two. Note that $\text{conv}_{c,k,m}$ with $m = 1$ does not result in any downsampling. Max-pooling usually results in a drastic reduction of the image size and by replacing it with a strided convolution, All-CNN achieves improved performance with much fewer parameters than many other networks on CIFAR-10. The final layer denoted as mean-pool takes the image of size $10 \times 8 \times 8$ and computes the spatial average to obtain an output vector of size 10. This network has $n = 1.67$ million parameters and is thus a medium-scale convolutional neural network as compared to other networks in the literature.

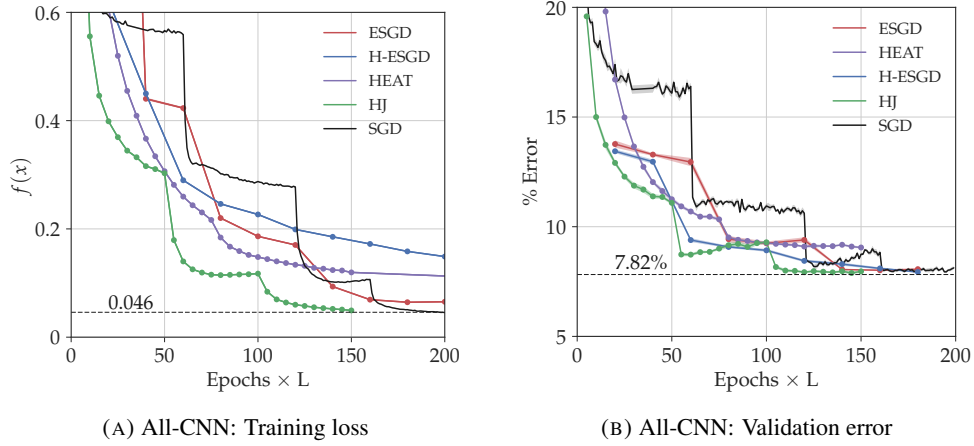


FIGURE 5. Training loss and validation error on CIFAR-10 (best seen in color)

Figure 5a and 5b show the training loss and validation error for the All-CNN network on the CIFAR-10 dataset. This is a more challenging classification task and H-ESGD obtains the best error of 7.82 % at 200 epochs. The Hamilton-Jacobi equation (HJ) obtains a comparable error (7.89 %) but converges much faster; moreover the training loss of HJ is the least among all the above algorithms while H-ESGD obtains a much higher training loss of 0.12. The other algorithms are close to each other in terms of both validation error and convergence rate for the networks considered here. Note however that all of them perform better than SGD. The heat equation is again an exception with a much higher validation error than others (9.04%). This is consistent with our discussion in Sec. 6.3 which suggests that the viscous or non-viscous HJ equations result in better smoothing than the heat equation.

Model	ESGD	HEAT	H-ESGD	HJ	SGD
mnistfc	1.08 \pm 0.02 @ 120	1.13 \pm 0.02 @ 200	1.15 \pm 0.03 @ 160	1.17 \pm 0.04 @ 200	1.10 \pm 0.01 @ 194
LeNet	0.5 \pm 0.01 @ 80	0.59 \pm 0.02 @ 75	0.51 \pm 0.02 @ 60	0.5 \pm 0.01 @ 70	0.5 \pm 0.02 @ 67
All-CNN	7.96 \pm 0.05 @ 160	9.04 \pm 0.04 @ 150	7.82 \pm 0.04 @ 200	7.89 \pm 0.07 @ 145	7.94 \pm 0.06 @ 195

TABLE 1. Summary of experimental results: Validation error (%) @ Effective epochs

9. DISCUSSION

Our results are steps towards grounding optimization of neural networks on established mathematical footings. In addition to helping explain effectiveness of state-of-the-art optimizers, the connections we establish also point the way to improving these algorithms.

The first practical implication is that, by solving the stochastic control problem corresponding to the viscous Hamilton-Jacobi PDE, we achieve a smaller expected loss compared to SGD; the improvement is an interpretable quantity, it is the action of the kinetic energy along the optimal path. The second is the equivalence of seemingly disparate methods such as Elastic-SGD and local entropy. This can help the development of distributed algorithms. Furthermore, our analysis provides an insight into the choice of hyper-parameters for these methods, which remains largely a black art in the practice of training deep networks. The third is that our analysis suggests more efficient algorithms, in particular, the fixed-point iteration derived from the non-viscous Hamilton-Jacobi equation. We thus simplify Entropy-SGD and improve its performance in practice, disentangle key parameters of the original algorithm such as scoping and thermal noise, and characterize its convergence properties.

Looking forward, while most PDEs achieve some kind of smoothing of their initial data, the properties that make the ones considered here tractable for deep learning and thereby inform further analyses in this direction are: (i) gradients of the solution can be computed using particle-based methods, e.g., an auxiliary SGD problem, and (ii) the results are

uniform in the coefficient of the viscosity. The former eliminates the need to compute the global solution of the PDE while the latter suggests that adding noise is not necessary to obtain a smoother landscape; indeed the best method in our paper is based on the non-viscous HJ equation.

10. ACKNOWLEDGMENTS

AO is supported by a grant from the Simons Foundation (395980); PC and SS by ONR N000141712072, AFOSR FA95501510229 and ARO W911NF151056466731CS; SO by ONR N000141410683, N000141210838, N000141712162 and DOE DE-SC00183838. AO would like to thank the hospitality of the UCLA mathematics department where this work was completed.

REFERENCES

- Baldassi, C., Borgs, C., Chayes, J., Ingrosso, A., Lucibello, C., Saglietti, L., and Zecchina, R. (2016a). Unreasonable effectiveness of learning neural networks: From accessible states and robust ensembles to basic algorithmic schemes. *PNAS*, 113(48):E7655–E7662.
- Baldassi, C., Ingrosso, A., Lucibello, C., Saglietti, L., and Zecchina, R. (2015). Subdominant dense clusters allow for simple learning and high computational performance in neural networks with discrete synapses. *Physical review letters*, 115(12):128101.
- Baldassi, C., Ingrosso, A., Lucibello, C., Saglietti, L., and Zecchina, R. (2016b). Local entropy as a measure for sampling solutions in constraint satisfaction problems. *Journal of Statistical Mechanics: Theory and Experiment*, 2016(2):023301.
- Baldi, P. and Hornik, K. (1989). Neural networks and principal component analysis: Learning from examples without local minima. *Neural Networks*, 2:53–58.
- Bauschke, H. H. and Combettes, P. L. (2011). *Convex analysis and monotone operator theory in Hilbert spaces*. Springer Science & Business Media.
- Bertsekas, D., Nedi, A., Ozdaglar, A., et al. (2003). Convex analysis and optimization.
- Bovier, A. and den Hollander, F. (2006). Metastability: A potential theoretic approach. In *International Congress of Mathematicians*, volume 3, pages 499–518.
- Bray, A. and Dean, D. (2007). The statistics of critical points of Gaussian fields on large-dimensional spaces. *Physics Review Letter*.
- Cannarsa, P. and Sinestrari, C. (2004). *Semiconcave functions, Hamilton-Jacobi equations, and optimal control*, volume 58. Springer Science & Business Media.
- Carrillo, J. A., McCann, R. J., and Villani, C. (2006). Contractions in the 2-wasserstein length space and thermalization of granular media. *Archive for Rational Mechanics and Analysis*, 179(2):217–263.
- Chaudhari, P., Choromanska, A., Soatto, S., LeCun, Y., Baldassi, C., Borgs, C., Chayes, J., Sagun, L., and Zecchina, R. (2016). Entropy-SGD: Biasing Gradient Descent Into Wide Valleys. *arXiv:1611.01838*.
- Chaudhari, P. and Soatto, S. (2015). On the energy landscape of deep networks. *arXiv:1511.06485*.
- Chen, X. (2012). Smoothing methods for nonsmooth, nonconvex minimization. *Mathematical programming*, pages 1–29.
- Chiang, T.-S., Hwang, C.-R., and Sheu, S. (1987). Diffusion for global optimization in \mathbb{R}^n . *SIAM Journal on Control and Optimization*, 25(3):737–753.
- Choromanska, A., Henaff, M., Mathieu, M., Ben Arous, G., and LeCun, Y. (2015). The loss surfaces of multilayer networks. In *AISTATS*.
- Coates, A., Lee, H., and Ng, A. Y. (2010). An analysis of single-layer networks in unsupervised feature learning. *Ann Arbor*, 1001(48109):2.
- Dauphin, Y., Pascanu, R., Gulcehre, C., Cho, K., Ganguli, S., and Bengio, Y. (2014). Identifying and attacking the saddle point problem in high-dimensional non-convex optimization. In *NIPS*.
- Defazio, A., Bach, F., and Lacoste-Julien, S. (2014). Saga: A fast incremental gradient method with support for non-strongly convex composite objectives. In *NIPS*.
- Duchi, J., Hazan, E., and Singer, Y. (2011). Adaptive subgradient methods for online learning and stochastic optimization. *JMLR*, 12:2121–2159.
- Evans, L. C. (1998). *Partial differential equations*, volume 19 of *Graduate Studies in Mathematics*. American Mathematical Society.
- Fleming, W. H. and Rishel, R. W. (2012). *Deterministic and stochastic optimal control*, volume 1. Springer Science & Business Media.
- Fleming, W. H. and Soner, H. M. (2006). *Controlled Markov processes and viscosity solutions*, volume 25. Springer Science & Business Media.
- Fyodorov, Y. and Williams, I. (2007). Replica symmetry breaking condition exposed by random matrix calculation of landscape complexity. *Journal of Statistical Physics*, 129(5-6):1081–1116.
- Geman, S. and Hwang, C.-R. (1986). Diffusions for global optimization. *SIAM Journal on Control and Optimization*, 24(5):1031–1043.
- Ghadimi, S. and Lan, G. (2013). Stochastic first- and zeroth-order methods for nonconvex stochastic programming. *SIAM Journal on Optimization*, 23(4):2341–2368.
- Gulcehre, C., Moczulski, M., Denil, M., and Bengio, Y. (2016). Noisy activation functions. In *ICML*.
- Haeffele, B. and Vidal, R. (2015). Global optimality in tensor factorization, deep learning, and beyond. *arXiv:1506.07540*.

- Huang, M., Malhamé, R. P., Caines, P. E., et al. (2006). Large population stochastic dynamic games: closed-loop McKean-Vlasov systems and the Nash certainty equivalence principle. *Communications in Information & Systems*, 6(3):221–252.
- Ioffe, S. and Szegedy, C. (2015). Batch normalization: Accelerating deep network training by reducing internal covariate shift. *arXiv:1502.03167*.
- Jordan, R., Kinderlehrer, D., and Otto, F. (1998). The variational formulation of the Fokker–Planck equation. *SIAM journal on mathematical analysis*, 29(1):1–17.
- Kingma, D. and Ba, J. (2014). Adam: A method for stochastic optimization. *arXiv:1412.6980*.
- Kramers, H. A. (1940). Brownian motion in a field of force and the diffusion model of chemical reactions. *Physica*, 7(4):284–304.
- Krizhevsky, A. (2009). Learning multiple layers of features from tiny images. Master’s thesis, Computer Science, University of Toronto.
- Krizhevsky, A., Sutskever, I., and Hinton, G. E. (2012). Imagenet classification with deep convolutional neural networks. In *NIPS*.
- Kushner, H. (1987). Asymptotic global behavior for stochastic approximation and diffusions with slowly decreasing noise effects: global minimization via Monte Carlo. *SIAM Journal on Applied Mathematics*, 47(1):169–185.
- Lasry, J.-M. and Lions, P.-L. (1986). A remark on regularization in Hilbert spaces. *Israel Journal of Mathematics*, 55(3):257–266.
- Lasry, J.-M. and Lions, P.-L. (2007). Mean field games. *Japanese Journal of Mathematics*, 2(1):229–260.
- LeCun, Y., Bengio, Y., and Hinton, G. (2015). Deep learning. *Nature*, 521(7553):436–444.
- LeCun, Y., Bottou, L., Bengio, Y., and Haffner, P. (1998). Gradient-based learning applied to document recognition. *Proceedings of the IEEE*, 86(11):2278–2324.
- Li, Q., Tai, C., et al. (2015). Dynamics of stochastic gradient algorithms. *arXiv:1511.06251*.
- Marshall, A. W., Olkin, I., and Arnold, B. C. (1979). *Inequalities: theory of majorization and its applications*, volume 143. Springer.
- Mezard, M., Parisi, G., and Virasoro, M. A. (1987). Spin glass theory and beyond.
- Mobahi, H. (2016). Training Recurrent Neural Networks by Diffusion. *arXiv:1601.04114*.
- Moreau, J.-J. (1965). Proximité et dualité dans un espace hilbertien. *Bulletin de la Société mathématique de France*, 93:273–299.
- Neal, R. (2011). MCMC using Hamiltonian dynamics. *Handbook of Markov Chain Monte Carlo*, 2:113–162.
- Nemirovski, A., Juditsky, A., Lan, G., and Shapiro, A. (2009). Robust stochastic approximation approach to stochastic programming. *SIAM Journal on optimization*, 19(4):1574–1609.
- Nesterov, Y. (1983). A method of solving a convex programming problem with convergence rate $O(1/k^2)$. In *Soviet Mathematics Doklady*, volume 27, pages 372–376.
- Oberman, A. M. (2006). Convergent difference schemes for degenerate elliptic and parabolic equations: Hamilton-Jacobi equations and free boundary problems. *SIAM J. Numer. Anal.*, 44(2):879–895 (electronic).
- Pavliotis, G. A. and Stuart, A. (2008). *Multiscale methods: averaging and homogenization*. Springer Science & Business Media.
- Risken, H. (1984). Fokker-planck equation. In *The Fokker-Planck Equation*, pages 63–95. Springer.
- Robbins, H. and Monro, S. (1951). A stochastic approximation method. *The annals of mathematical statistics*, pages 400–407.
- Robert, C. and Casella, G. (2013). *Monte Carlo statistical methods*. Springer Science & Business Media.
- Rockafellar, R. T. (1976). Monotone operators and the proximal point algorithm. *SIAM journal on control and optimization*, 14(5):877–898.
- Rumelhart, D. E., Hinton, G. E., and Williams, R. J. (1988). Learning representations by back-propagating errors. *Cognitive modeling*, 5(3):1.
- Sagun, L., Bottou, L., and LeCun, Y. (2016). Singularity of the Hessian in Deep Learning. *arXiv:1611.07476*.
- Santambrogio, F. (2015). Optimal transport for applied mathematicians. *Birkhäuser, NY*.
- Saxe, A., McClelland, J., and Ganguli, S. (2014). Exact solutions to the nonlinear dynamics of learning in deep linear neural networks. In *ICLR*.
- Schmidt, M., Le Roux, N., and Bach, F. (2013). Minimizing finite sums with the stochastic average gradient. *Mathematical Programming*, pages 1–30.
- Schur, I. (1923). Über eine Klasse von Mittelbildungen mit Anwendungen auf die Determinantentheorie. *Sitzungsberichte der Berliner Mathematischen Gesellschaft*, 22:9–20.
- Soudry, D. and Carmon, Y. (2016). No bad local minima: Data independent training error guarantees for multilayer neural networks. *arXiv:1605.08361*.
- Springenberg, J., Dosovitskiy, A., Brox, T., and Riedmiller, M. (2014). Striving for simplicity: The all convolutional net. *arXiv:1412.6806*.
- Srivastava, N., Hinton, G., Krizhevsky, A., Sutskever, I., and Salakhutdinov, R. (2014). Dropout: a simple way to prevent neural networks from overfitting. *JMLR*, 15(1):1929–1958.
- Szegedy, C., Liu, W., Jia, Y., Sermanet, P., Reed, S., Anguelov, D., Erhan, D., Vanhoucke, V., and Rabinovich, A. (2015). Going deeper with convolutions. In *CVPR*.
- Welling, M. and Teh, Y. W. (2011). Bayesian learning via stochastic gradient Langevin dynamics. In *ICML*.
- Zhang, S., Choromanska, A., and LeCun, Y. (2015). Deep learning with elastic averaging SGD. In *NIPS*.